J. Fluid Mech. (1978), *vol.* 88, *part* 4, *pp.* 737–756
Printed in Great Britain

The plane turbulent impinging jet

By E. GUTMARK, M. WOLFSHTEIN
Department of Aeronautical Engineering, Technion – Israel Institute of Technology, Haifa
AND I. WYGNANSKI
School of Engineering, Tel-Aviv University, Ramat-Aviv, Israel

(Received 14 September 1976 and in revised form 6 April 1978)

This paper presents an experimental study of the turbulent structure on the centre-line of a two-dimensional impinging jet. The mean velocity, turbulent stresses, triple velocity products and temporal derivatives were measured and the energy balances for the three fluctuating components were calculated. The results indicate a selective stretching of vortices in the direction in which the streamlines spread near the wall, causing anisotropy in this region. The distribution of energy among various frequencies was found from spectral measurements. These measurements revealed the existence of a neutral frequency above which the energy was attenuated by viscous dissipation and below which it was augmented by a vortex-stretching mechanism.

1. Introduction

The present paper describes an experimental investigation of the turbulent impinging jet. This flow is of considerable theoretical interest because the diverging streamlines upstream of impingement stretch the eddies whose axes are parallel to the direction of stretching and whose scales are sufficiently large to prevent viscous dissipation from dominating the process. The redistribution of the turbulent energy in the three principal directions by the pressure–velocity correlations is also of interest.

The augmentation of turbulence in the stagnation region is coupled with an increase in heat transfer to or from the flow and can be used in some important engineering applications. Therefore the impinging jet has been investigated experimentally by many researchers. Some of these investigators studied the flow field in detail. The mean velocity on the centre-line of a two-dimensional impinging jet was measured by Schauer & Eustis (1963) and by Beltaos & Rajaratnam (1973). Donaldson, Snedeker & Margolis (1971) measured the mean velocity and the three components of the turbulent fluctuations on the axis of a circular impinging jet in addition to making some measurements of pressure fluctuations and heat transfer on the impingement plate. Gardon & Akfirat (1965) noted that the level of turbulence in the jet has a significant effect on the rate of heat transfer between the impingement plate and the jet. The many papers which are concerned only with measurements of heat and mass transfer by impinging jets will not be cited here.

In an early account of stagnation flow, Kestin & Maeder (1957) observed a substantial augmentation of heat-transfer rates in the stagnation region of a circular cylinder when the level of ambient turbulence was increased. Smith & Kuethe (1966) measured the heat transfer and skin friction in the stagnation region of a circular

cylinder and a flat plate. They also reported augmentation of the heat transfer and skin friction, which they were able to relate theoretically to the turbulence intensity in the oncoming stream. Sutera, Maeder & Kestin (1963) hypothesized that the augmentation of turbulence intensity is caused by stretching of those vortices whose axes are normal to the plane of symmetry. The impinging jet is somewhat similar to stagnation flow, in which an infinite stream impinges on a finite body. Studying the development of spatially undulating, steady, laminar flow, Sutera *et al.* identified a neutral scale which separated the small vortices dominated by dissipation from the larger vortices whose energy is augmented by the stretching mechanism. Sadeh, Sutera & Maeder (1970) extended these calculations to the flow field outside the viscous layer and measured some turbulent properties in this region. They found an appreciable augmentation of the turbulence in the stagnation region and related this augmentation to the structure of the impinging turbulence. Another interesting feature reported by these authors is the discovery of stationary eddies near the wall. Bearman (1972) studied experimentally the distortion of grid-generated turbulence in the stagnation region of a two-dimensional bluff body. His results indicated that the small eddies decay while the large ones increase in intensity. The augmentation of turbulence may be explained by the rapid-distortion theory of Batchelor & Proudman (1954), which was applied by Hunt (1973) to stagnation flow. This theory is applicable to fairly weak, large-scale turbulence. In the present experiments only the lowest frequencies fall in this category.

The purpose of this paper is threefold: (i) to investigate the stretching mechanism of the turbulent eddies and its dependence on eddy scale; (ii) to study the components of the turbulent energy balance; (iii) to document the flow characteristics on the centre-line of the plane impinging jet.

2. Experimental set-up

2.1. *Experimental apparatus and procedure*

The jet emerged from a nozzle 1·3 cm wide and 50 cm long (figure 1). The flow velocity at the exit was 35 m/s and the Reynolds number based on the nozzle width was 30 000. The plate on which the jet impinged was installed 100 slot widths downstream of the nozzle, at right angles to the jet. The plate was pressure tapped in order to check the symmetry of the flow.

All the velocity measurements were done using DISA hot-wire anemometers and conventional analog equipment for signal processing. To facilitate measurements in the immediate vicinity of the wall, the probe was inserted through a small hole in the plate. The hole was sealed during the tests in order to minimize the disturbances to the flow.

All the results were corrected for the high intensity of turbulence using the response equation derived by Heskestad (1965, equations 46, 48, 23–29, 36–39, pp. 728, 730). The yaw sensitivity of the probes was obtained by direct calibration, thus accounting for tangential cooling (Champagne & Sleicher 1967).

2.2. *Non-dimensional presentation of results*

The characteristic length and velocity scales of the problem are the centre-line velocity of the jet and its local width upstream of the stagnation region. However, since these

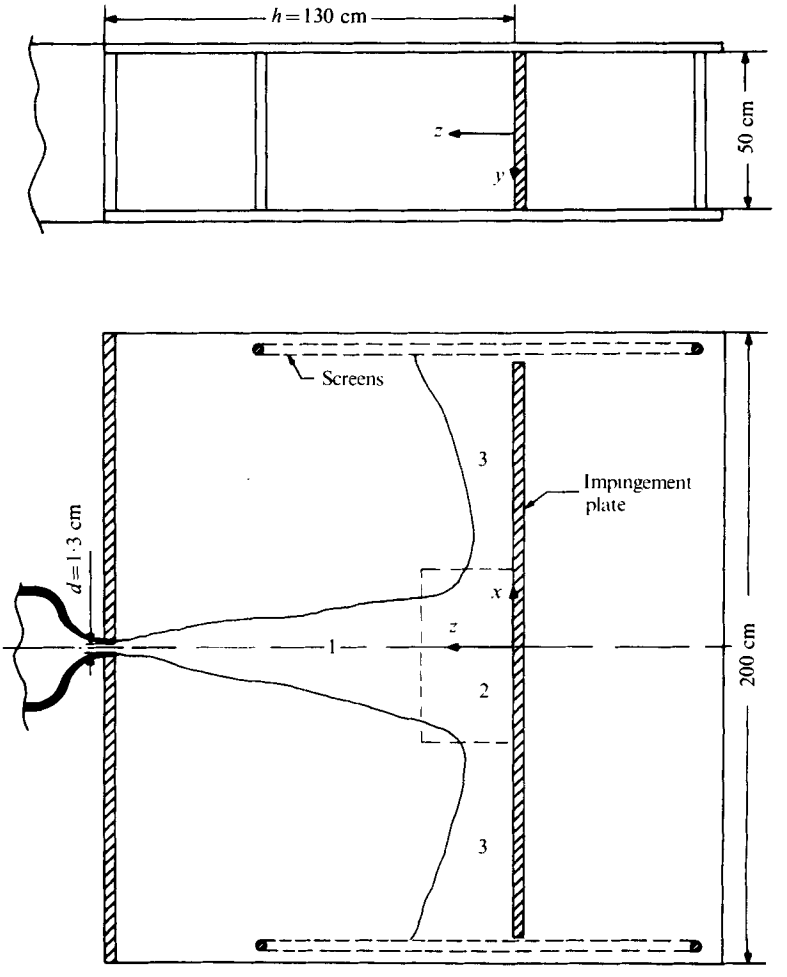

FIGURE 1. Schematic diagram of experimental apparatus. (1) Free-jet zone. (2) Stagnation zone. (3) Wall-jet zone.

quantities are not known we used the length and velocity scales which would have existed at the stagnation plane had the plate been removed. These are given by

$$W_{\max,s}/W_0 \propto (d/h)^{\frac{1}{2}}, \quad \delta_s/d \propto h/d,$$

where h is the distance from the plate to the nozzle, d is the width of the nozzle and W_0 is the exit velocity. Thus the scaling parameters for the velocity and the length scale were $W_0(d/h)^{\frac{1}{2}}$ and h respectively. Obviously, distances should be measured from the stagnation plate and not from the nozzle. In principle h should be measured from the virtual origin of the jet, however at $h/d = 100$ the difference is small. Some frequencies were rendered dimensionless in terms of the Strouhal number

$$St = \frac{fh}{W_0}\left(\frac{h}{d}\right)^{\frac{1}{2}},$$

where f is the frequency.

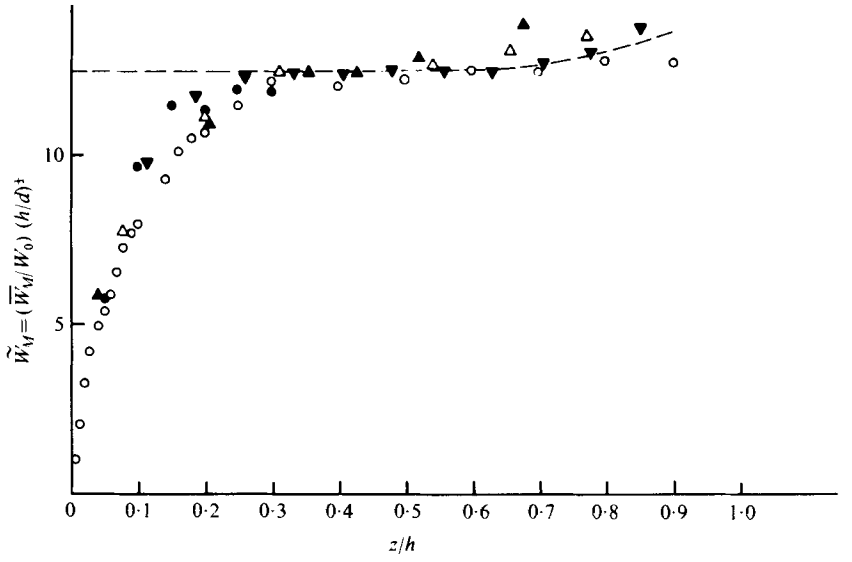

FIGURE 2. The mean longitudinal velocity along the jet centre-line. ○, present measurements, $Re = 3 \times 10^4, h/d = 100$; ●, Schauer & Eustis (1963), $Re = 4{\cdot}3 \times 10^4, h/d = 40$; ▲, △, ▼, Beltaos & Rajaratnam (1973), $Re = 5{\cdot}6 \times 10^3$, $h/d = 31$, 43·6, 67·5; ---, plane free jet, Gutmark & Wygnanski (1976), $Re = 3 \times 10^4, h/d = 100$.

3. Results and discussion

3.1. *Mean velocity*

The mean longitudinal component of velocity, $\overline{W}_M$, was measured using an X-wire. In figure 2 the dimensionless quantity $(\overline{W}_M/W_0)(h/d)^{\frac{1}{2}}$ is plotted *vs.* the dimensionless length z/h. Other sets of data are shown as well. Schauer & Eustis (1963) measured the velocity distribution along the centre-line of a plane impinging jet but in their case the distance between the nozzle and the plate was 40 slot widths, while Beltaos & Rajaratnam (1973) studied the same flow for h/d varying between 30 and 70. The agreement of the three sets of data is good, in spite of the different Reynolds numbers and h/d ratios. Thus it may be concluded that the normalizing quantities were properly selected. Near the wall there is a region where the velocity is proportional to the distance from the wall. This linear relation is characteristic of inviscid stagnation flows. In the case of the impinging jet this region is limited to the immediate neighbourhood of the plate.

In order to estimate the extent of the upstream influence of the stagnation plate on the mean flow, the velocity decay of the impinging jet is compared with the free-jet data reported by Gutmark & Wygnanski (1976). The deviation from a free jet does not extend further than $z/h = 0{\cdot}2$ (i.e. 20 % of the distance between the plate and the origin of the jet). At this point the characteristic width of the jet is $x_{\frac{1}{2}m} = 0{\cdot}07\,h$, where, at a given z, $x_{\frac{1}{2}m}$ is the distance from the centre-line of the jet to the location at which the velocity is equal to half the velocity on the centre-line (Gutmark & Wygnanski 1976).

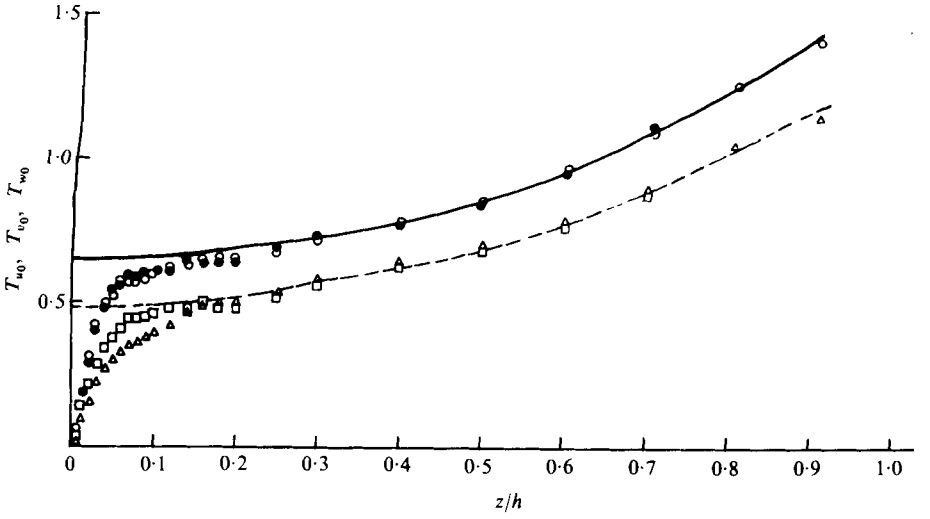

FIGURE 3. The three fluctuating velocity components along the jet centre-line. Present results: ●, T_{w_0}, z, y plane; ○, T_{w_0}, z, x plane; △, T_{u_0}; □, T_{v_0}. Plane free jet (Gutmark & Wygnanski 1976): ——, T_{w_0}; – – –, T_{u_0}, T_{v_0}.

3.2. *The fluctuation intensities*

Figure 3 shows the r.m.s. values of the three components of the velocity fluctuations properly normalized:

$$T_{u_0} = \frac{(\overline{u'^2})^{\frac{1}{2}}}{W_0(d/h)^{\frac{1}{2}}}, \quad T_{v_0} = \frac{(\overline{v'^2})^{\frac{1}{2}}}{W_0(d/h)^{\frac{1}{2}}}, \quad T_{w_0} = \frac{(\overline{w'^2})^{\frac{1}{2}}}{W_0(d/h)^{\frac{1}{2}}}.$$

The longitudinal fluctuations were measured twice, with the wires in the z, x and z, y planes respectively. There is no significant difference between the two sets of measurements of T_{w_0}. The distributions of the three fluctuating velocity components in the impinging jet are compared with the corresponding values in the free jet. Both flows exhibit the same behaviour up to a distance of about $0{\cdot}15\,h$ from the stagnation line. Downstream of this point, the influence of the wall appears to be very anisotropic. Thus the lateral component T_{u_0} initially decays much faster than the other two components, which do not seem to be affected by the presence of the wall until a distance of $0{\cdot}07\,h$ from the wall. Downstream of this point T_{w_0} and T_{v_0} decrease rapidly to zero at the wall. This behaviour is attributed to the stretching of vortex lines in the x direction and compression of vortex lines in the z direction. It is expected that the stretching will enhance the intensity of v' and w' while the compression will attenuate u' and v'. Unlike the results of Sadeh *et al.*, the absolute intensity of the turbulence does not increase, but the ratio of the turbulent fluctuations to the local velocity $\overline{W}_M$ does increase, as seen in figure 4. (Both $(\overline{w'^2})^{\frac{1}{2}}/\overline{W}_M$ and $(\overline{v'^2})^{\frac{1}{2}}/\overline{W}_M$ increase faster than $(\overline{u'^2})^{\frac{1}{2}}/\overline{W}_M$.)

3.3. *Spectral distribution of the energy components*

In order to permit a better understanding of the structure of the turbulence of the impinging jet, the energy spectra of u', v' and w' were measured at seven stations located at distances ranging from $0{\cdot}025\,h$ to $0{\cdot}4\,h$ from the stagnation plate. These measurements were made with a Dytronics Filter (Model 720) with a window width equal to 7 % of the centre-frequency. The use of a digital spectrum analyser (Saicor, Model

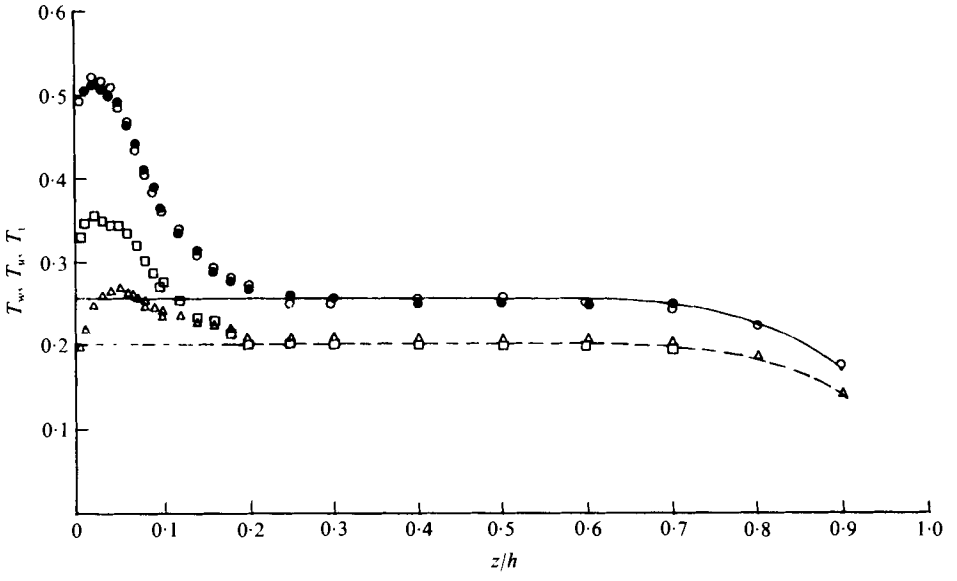

FIGURE 4. The three turbulence intensity components along the jet centre-line. Present results: ●, $T_w = (\overline{w'^2})^{\frac{1}{2}}/\overline{W}_M, z, y$ plane; ○, T_w, z, x plane; △, $T_u = (\overline{u'^2})^{\frac{1}{2}}/\overline{W}_M$; □, $T_v = (\overline{v'^2})^{\frac{1}{2}}/\overline{W}_M$. Plane free jet (Gutmark & Wygnanski 1976): ——, T_w; – – –, T_u, T_v.

SAI-52B) with a constant window width did not change the results. The spectral distributions are so normalized that the area under the spectral curves is equal to the corresponding intensity, e.g.

$$T_{w_0} = \int_0^\infty F_z(f)\,df.$$

It is interesting to note that the spectral distributions F_z and F_y both have a region in which the slope is $-\frac{5}{3}$, in spite of the anisotropic stretching.

The distributions of F_z and F_y (figures 5*a*, *b*) 'cross over' at frequencies of 5·6 and 3·0 respectively, where most spectral curves intersect. We shall henceforth define the cross-over point as a 'neutral' frequency. This frequency is probably dependent on the distance between the plate and the nozzle. Above the neutral frequency, the intensity of the fluctuations is reduced as the impingement plate is approached, while the opposite occurs below the neutral frequency. There is no cross-over in the u' spectral distribution F_x (figure 5*c*). The neutral frequency of F_z is probably associated with the dissipation-dominated part of the spectrum.

The concentration of the x component of intensity between $St = 3$ and $St = 10$ (see figure 5*c*) is believed to correspond to the largest eddies which can exist under the restraining influence of the finite width of the jet. This width should be approximately 40 cm at $z/h = 0{\cdot}2$ (Gutmark & Wygnanski 1976) and when divided by the appropriate velocity scale gives $St = 7$. The shape of the spectral distributions shown in figure 5(*c*) for $z/h > 0{\cdot}1$ suggest that eddies of a preferred size pile up against the plate before being strained by the mean flow field in the immediate vicinity of the stagnation line.

The v' spectra (figure 5*b*) also peak at $3 < St < 15$ but this peak can only be attributed to the characteristic length scale of the experimental apparatus, i.e. the distance between the upper and lower bounding end plates. The F_z spectrum (figure 5*a*) is rather

flat in the low frequency range because there is no obvious mechanism which will tend to limit the size of the eddies in the x direction. The characteristic length scale in the direction of these eddies is the distance between the nozzle and the plate, which is rather large in the present study. If this distance were to become comparable to the length of the potential core (i.e. $h/d < 10$) the results might be quite different as one would expect the flow to lock onto one of the preferred frequencies which are known to dominate the core region.

3.4. *Energy components at different frequencies*

The power spectra of the different components of the turbulent intensity suggest that the amplification and decay processes are frequency dependent. This becomes obvious when the energy content of each component of the turbulent intensity at a specific frequency is followed along the axis of the jet. The results for some representative frequencies in the range $2 < St < 37$ are shown in figures 6 (*a*)–(*c*).

The most amplified scale in the z direction (figure 6*a*) occurs at the lowest frequency reported ($St = 2{\cdot}6$) at $z/h = 0{\cdot}12$. At this point the intensity has increased by more than a factor of two in comparison with the value that would have existed in absence of the plate. For $z/h < 0{\cdot}12$ the intensity of the large scales starts to decay. A neutral scale which does not undergo amplification as the flow approaches stagnation exists. The frequency corresponding to this scale is $St_{0z} = 5{\cdot}6$. Smaller-scale eddies decay even at $z/h \approx 0{\cdot}25$. Very close to the plate ($z/h < 0{\cdot}1$) the intensity of the w' component diminishes as the flow approaches stagnation for all eddy scales considered.

The turbulent energy content in the y direction (figure 6*b*) is much smaller than F_z at all scales. This is not surprising, since F_y is not generated directly in this flow and is sustained only by transport from the upstream region and by redistribution of energy. The neutral frequency for this component is approximately $St_{0y} = 3$ and the energy contained in this frequency is low. Absolute intensification of energy is seen only for $St = 2$ for $z/h < 0{\cdot}1$. Because of the two-dimensional nature of the mean flow, changes in the energy-containing eddies are small.

The lateral energy distribution F_x (figure 6*c*) differs from the other two components. The fast decay of the mean velocity near the plate gives rise to negative production of u', which therefore decays very rapidly for $z/h < 0{\cdot}2$. This behaviour is most apparent in the large eddies which are strained by the mean flow.

3.5. *Two-point double velocity correlations*

The longitudinal correlation coefficient at any point in the jet is defined by

$$R_{33}(0,0,\Delta z) = \frac{\overline{w'(z)\,w'(z+\Delta z)}}{[\overline{w'^2(z)}]^{\frac{1}{2}}\,[\overline{w'^2(z+\Delta z)}]^{\frac{1}{2}}},$$

the lateral correlation coefficient is

$$R_{33}(\Delta x,0,0) = \frac{\overline{w'(\frac{1}{2}\Delta x)\,w'(-\frac{1}{2}\Delta x)}}{[\overline{w'^2(\frac{1}{2}\Delta x)}]^{\frac{1}{2}}\,[\overline{w'^2(-\frac{1}{2}\Delta x)}]^{\frac{1}{2}}}$$

and the transverse correlation is

$$R_{33}(0,\Delta y,0) = \frac{\overline{w'(\frac{1}{2}\Delta y)\,w'(-\frac{1}{2}\Delta y)}}{[\overline{w'^2(\frac{1}{2}\Delta y)}]^{\frac{1}{2}}\,[\overline{w'^2(-\frac{1}{2}\Delta y)}]^{\frac{1}{2}}}.$$

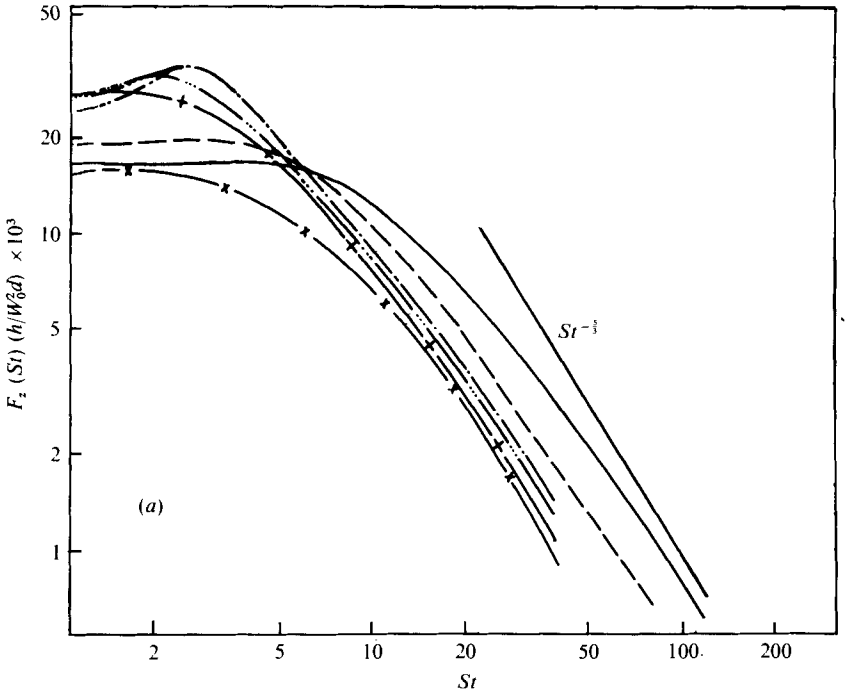

FIGURE 5 (*a*). For legend see facing page.

$R_{33}(0, 0, \Delta z)$ was measured by keeping one probe stationary and moving the other one in the upstream direction; to obtain $R_{33}(\Delta x, 0, 0)$ and $R_{33}(0, \Delta y, 0)$ both probes were moved an equal distance from the point at which the correlation distributions were measured. The central points of all correlations measured were on the centre-plane of the jet, at various distances from the stagnation plate.

The longitudinal correlation coefficient $R_{33}(0, 0, \Delta z)$ is similar to that of the free jet for $z/h > 0{\cdot}1$ (figure 7*a*). Closer to the plate the correlation curves become narrower as a result of the vortex stretching and distortion. The negative dip in the lateral correlation $R_{33}(\Delta x, 0, 0)$ which exists in all free jets and wakes (see curves for $\Delta x/(h-z) > 0{\cdot}06$) disappears entirely in this flow at $z/h = 0{\cdot}05$ (figure 7*b*). The strength of the negative dip is sometimes attributed to the influence of large eddies on opposite sides of the jet on the centre-line flow, because whenever the correlations are measured away from the centre-line, the negative dip diminishes and disappears. In this flow the dip disappears on the centre-line because the region from which these eddies derive their energy (i.e. where $\partial w/\partial x$ is maximum) moves away from the centre-line as the plate is approached. The rapid increase in the width of the jet causes a corresponding increase in the integral scale.

The third correlation $R_{33}(0, \Delta y, 0)$, plotted in figure 7(*c*), behaves in much the same way as $R_{33}(0, 0, \Delta z)$, retaining its self-preserving nature up to a distance of $0{\cdot}1\,h$ from the stagnation plate. For $z/h < 0{\cdot}1$ the correlation length diminishes because the jet becomes wider and those eddies which are not directly stretched by the mean flow may simply be displaced, reducing the correlation coefficient.

The correlation length in the y direction is $\Delta y/(h-z) \sim 0{\cdot}07$. The ratio of the distance

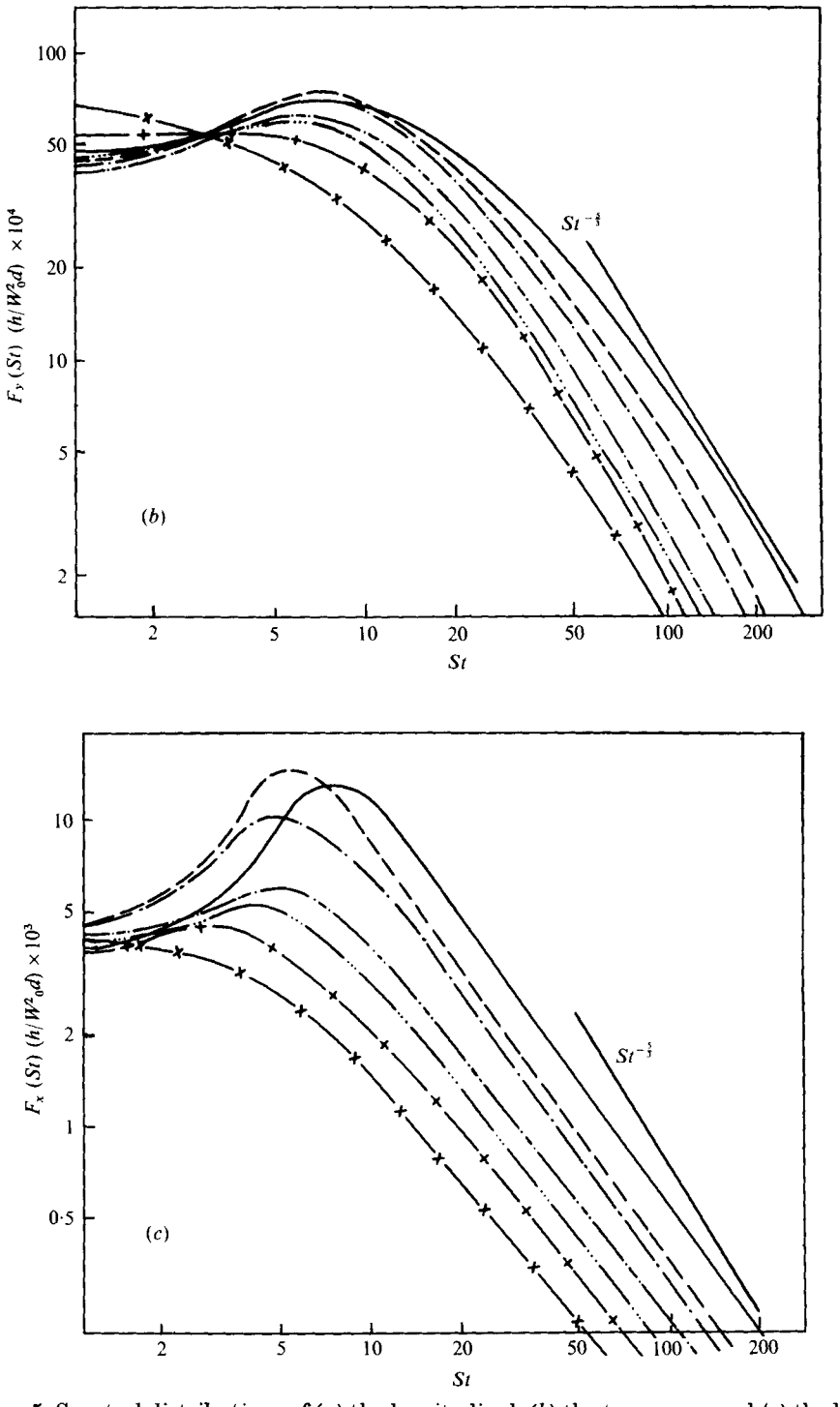

FIGURE 5. Spectral distributions of (*a*) the longitudinal, (*b*) the transverse and (*c*) the lateral velocity fluctuations along the jet centre-line. ——, $z/h = 0{\cdot}4$; – – –, $z/h = 0{\cdot}21$; — · —, $z/h = 0{\cdot}15$; —·· · ··—, $z/h = 0{\cdot}096$; — · · · —, $z/h = 0{\cdot}075$; —+—, $z/h = 0{\cdot}05$; —×—, $z/h = 0{\cdot}025$.

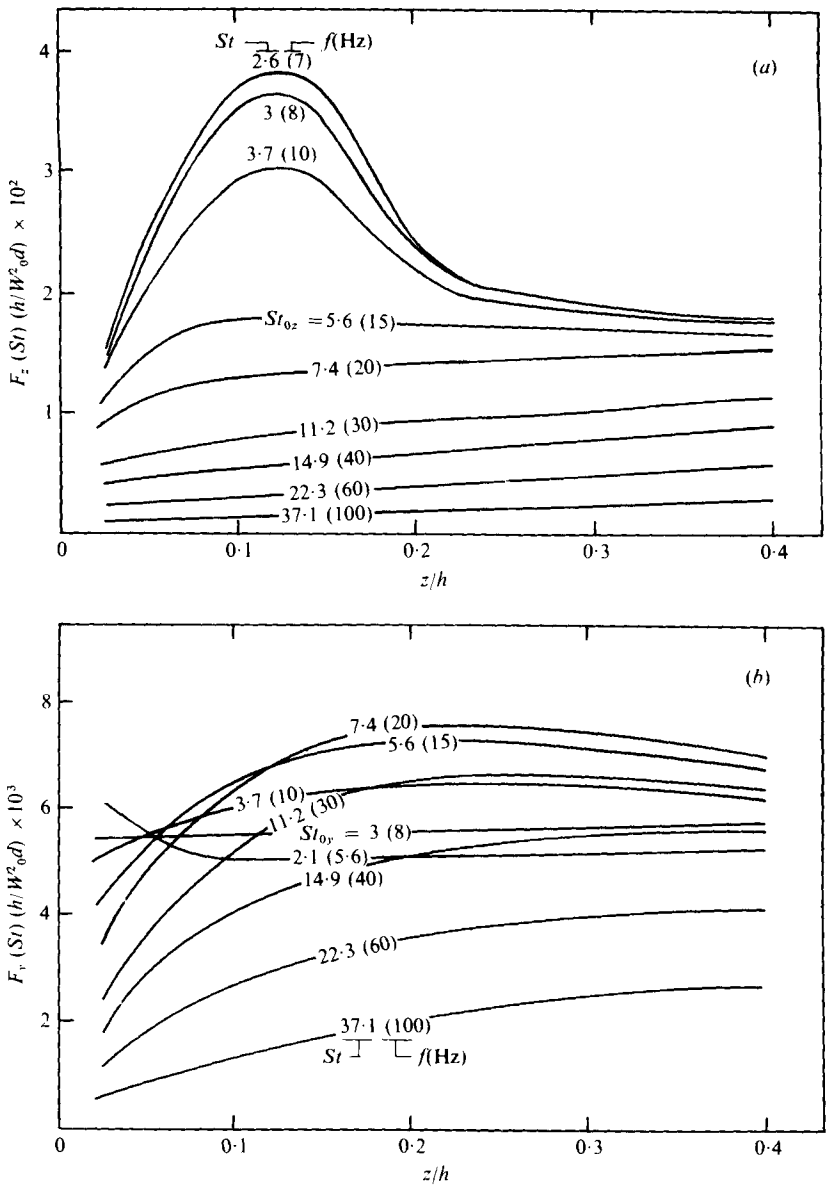

FIGURES 6 (*a*, *b*). For legend see facing page.

between the two confining horizontal walls to $h-z$ is 0·4. Therefore the distance between the walls is about six times the integral scale, implying that the aspect ratio is high enough to provide two-dimensionality of the mean flow in the y direction. In other words, the effect of the walls on all but the largest eddies in the jet is expected to be negligible.

The lack of periodicity in the correlations $R_{33}(0, 0, \Delta z)$ and $R_{33}(0, \Delta y, 0)$ indicates that a standing vortex pattern as described by Sadeh *et al.* (1970) does not exist in the flow. A quasi-regular pattern of discrete vortices, oscillating slowly in time, may still exist, but it cannot be detected by conventional methods.

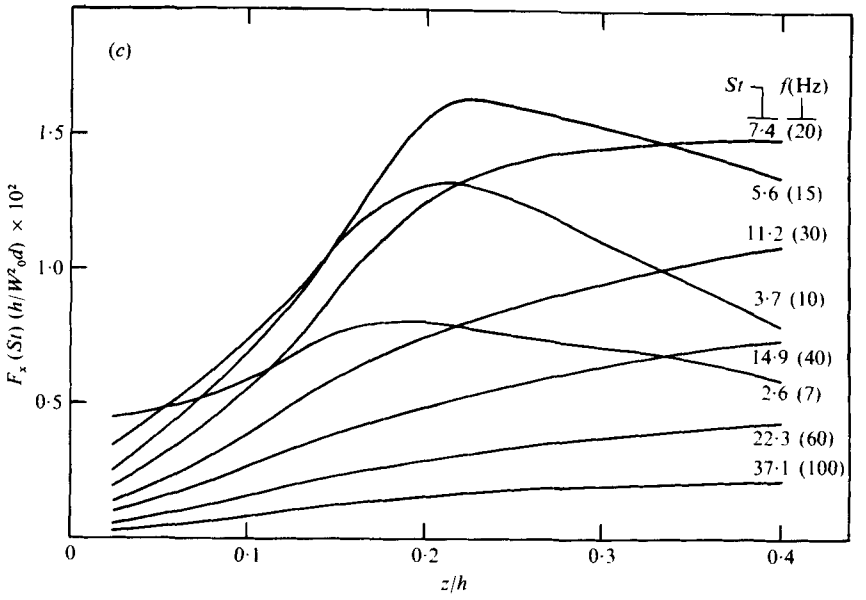

FIGURE 6. (*a*) Longitudinal, (*b*) transverse and (*c*) lateral velocity fluctuations at different frequencies along the jet centre-line. (*a*) $St_{0z} = 5{\cdot}6, f_{0z} = 15\,\text{Hz}, \lambda_{0z}(z/h = 0{\cdot}1) = 0{\cdot}4\,\text{m}$. (*b*) $St_{0v} = 3$, $f_{0v} = 8\,\text{Hz}$, $\lambda_{0v}(z/h = 0{\cdot}1) = 0{\cdot}75\,\text{m}$. (*c*) No neutral frequency identified.

3.6. *The dissipation derivatives and microscales*

The dissipation of turbulent energy is approximated by

$$\nu \sum_{i,j=1,2,3} \overline{(\partial u_i'/\partial x_j)^2}.$$

Taylor's hypothesis was used to transform the temporal derivatives to spatial derivatives in the z direction. The transformed derivatives were corrected to account for the high intensity of turbulence (Heskestad 1965). Other derivatives were not measured. The three derivatives are plotted in figure 8 as a function of the distance from the stagnation surface. Far away from the plate, $\overline{(\partial v'/\partial z)^2}$ and $\overline{(\partial u'/\partial z)^2}$ are equal to and higher than $\overline{(\partial w'/\partial z)^2}$. In the stagnation region, however, $\overline{(\partial w'/\partial z)^2}$ increases much more rapidly than the other derivatives, becoming the strongest source of dissipation at $z/h < 0{\cdot}06$. Since most of the turbulent energy in the stagnation zone is also concentrated in the w component one expects that the dissipation will follow suit. Indeed the Taylor microscales, which represent ratios of the dimensions of the energy-containing eddies to those of the dissipation eddies, behave in much the same way for both the longitudinal and lateral components (figure 9). The microscale λ_z is approximately 1·5 times larger than λ_x. Both scales grow linearly in the free-jet region but when the wall is approached they reach their maximum values at $z/h = 0{\cdot}15$. From this point on the microscales decrease monotonically towards the wall.

3.7. *Integral scales*

The integral scales were calculated by integration of the two-point correlation distributions. Their respective definitions are

$$\Lambda_z = \int_0^\infty R_{33}(0,0,\Delta z)\,dz, \quad \Lambda_x = \int_0^\infty R_{33}(\Delta x,0,0)\,dx, \quad \Lambda_y = \int_0^\infty R_{33}(0,\Delta y,0)\,dy.$$

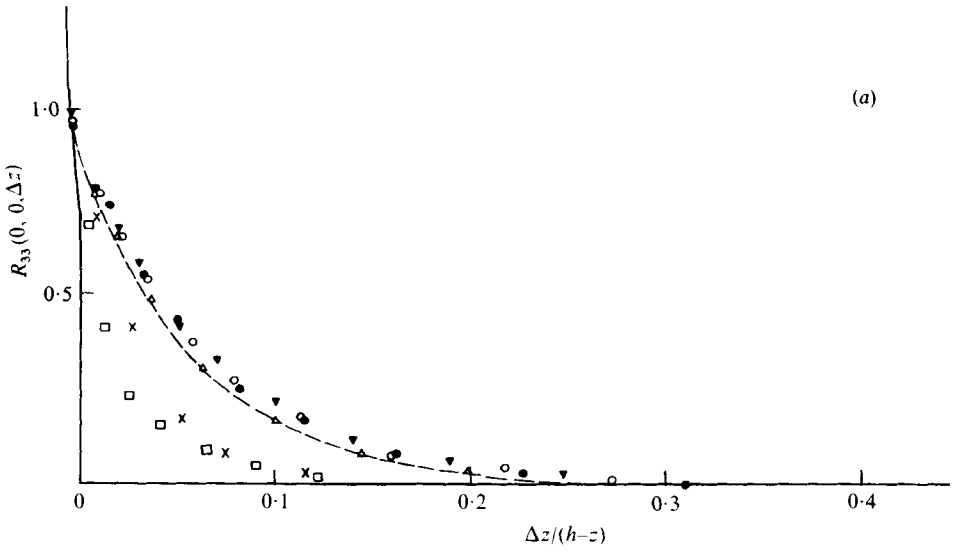

FIGURE 7 (a). For legend see facing page.

The three scales are plotted in figure 10. It should be noted that calculation of Λ_x from the above definition yields misleading results as the negative and positive parts of the two-point correlation ($R_{33}(\Delta x, 0, 0)$) tend to cancel one another. Therefore Λ_x was calculated in two ways: (i) by taking the integral of the positive part only and (ii) by summing the positive part and the absolute value of the negative part. Both lines are depicted in figure 10. However, only the second one takes full account of the larger eddies or the distance at which their influence is being felt and hence it was used in all subsequent discussions.

The scales Λ_z and Λ_x increase in the free-jet region until they attain a maximum at $z/h = 0{\cdot}15$. In the region $0{\cdot}05 < z/h < 0{\cdot}15$, Λ_z and Λ_x decrease rapidly as the wall is approached. The effect of the wall on Λ_y does not extend as far away from the wall as the effect on Λ_z and Λ_x (figure 10). Λ_y attains a maximum value at $z/h = 0{\cdot}1$ and only then decreases towards the wall.

At this point it is appropriate to consider the interpretation of the experimental results in the light of Hunt's (1973) theory. A detailed comparison of the present results with the theory of Hunt is not realistic because Hunt's calculations are limited to eddies which are either very large or very small in comparison with a typical dimension of a bluff body. Neither is true in the case of the impinging jet.

The typical length scale of the stagnation region in this case is $0{\cdot}2\,h$ and a typical integral scale at the beginning of the straining process (at $z/h = 0{\cdot}2$) is

$$\Delta z = 0{\cdot}06(h-z) = 0{\cdot}06h(1-z/h) = 0{\cdot}048h,$$

therefore the ratio between these two scales is 4·2. However, the integral scale is biased towards the large eddies in the flow, which do not contain most of the turbulent energy. If one compares time scales, then the mean-flow distortion time scale is $0{\cdot}2h/\overline{W}_M$ while the turbulent time scale is $\Delta z/(\overline{w'^2})^{\frac{1}{2}}$, which changes the length ratio by a factor

$$(\overline{w'^2})^{\frac{1}{2}}/\overline{W}_M = T_w(z/h = 0{\cdot}2) \approx 0{\cdot}25.$$

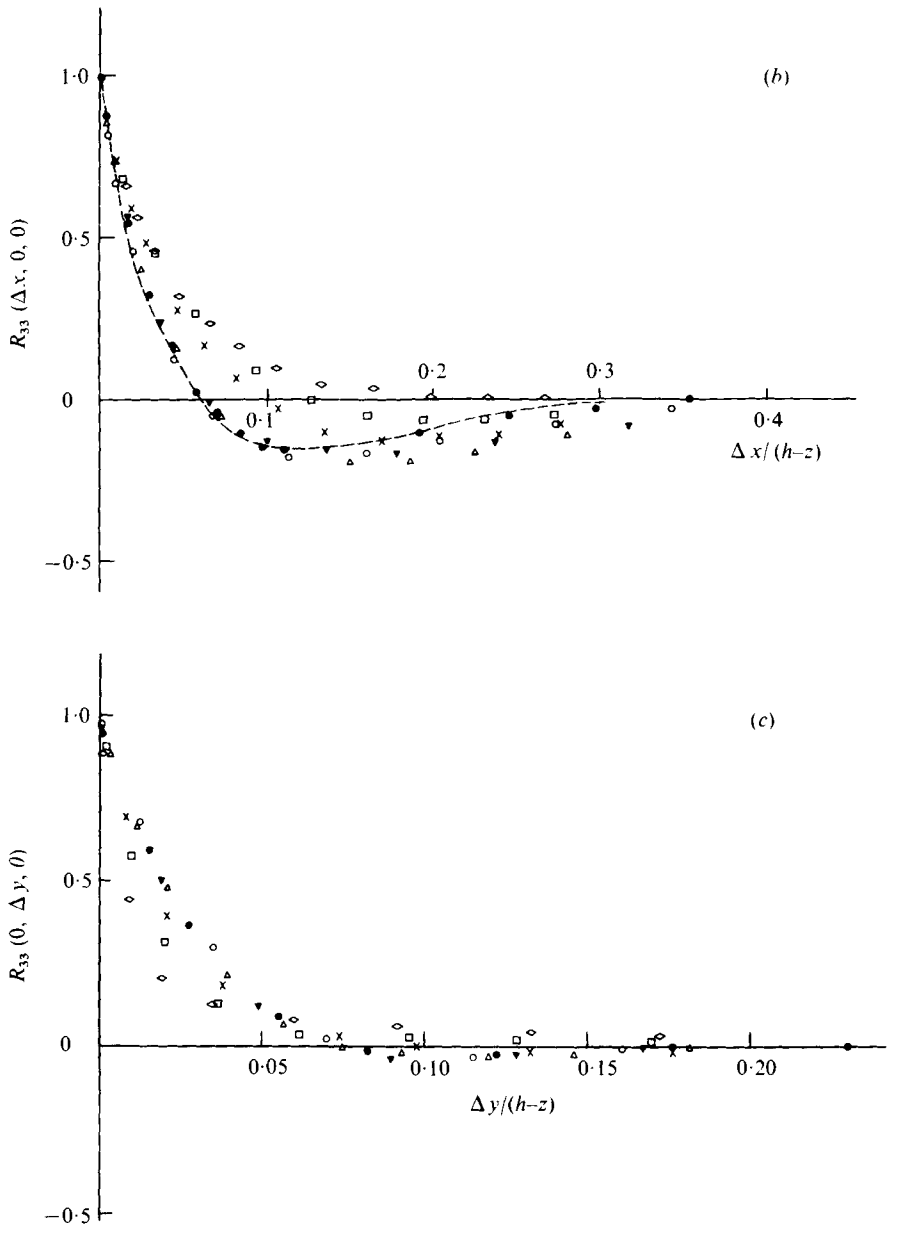

FIGURE 7. (*a*) Longitudinal, (*b*) lateral and (*c*) transverse correlation coefficients along the jet centre-line. – – –, plane free jet (Gutmark & Wygnanski 1976), (*a*) 78*d* and (*b*) 70*d* from the nozzle.

			●	○	▼	△	×	□	◇
(*a*)	z/h		0·5	0·3	0·2	0·1	0·05	0·02	—
	$\Lambda_z/(h-z)$		0·0602	0·0602	0·0602	0·0503	0·0298	0·0201	—
(*b*)	z/h		0·4	0·3	0·2	0·15	0·10	0·075	0·05
	$\Lambda_x/(h-z)$	positive area	0·0454	0·0546	0·0662	0·0662	0·0532	0·0462	0·0419
		+ |negative area|							
		positive area	0·0226	0·0226	0·0226	0·0226	0·0319	0·0370	0·0419
(*c*)	z/h		0·4	0·3	0·2	0·114	0·08	0·05	0·025
	$\Lambda_y/(h-z)$		0·0251	0·0251	0·0251	0·0251	0·0216	0·0195	0·0170

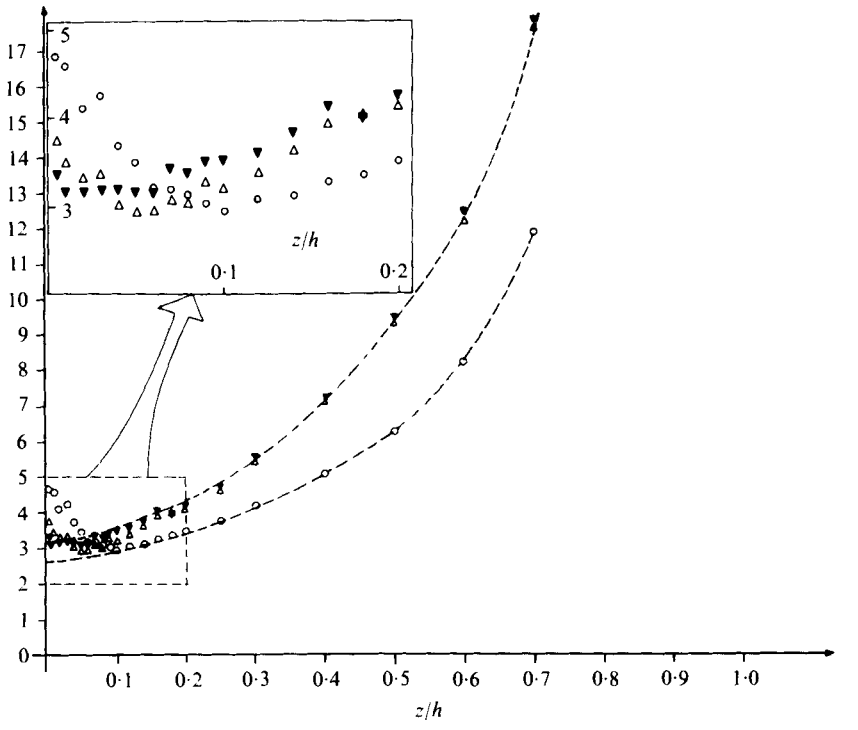

FIGURE 8. Dissipation derivatives along the jet centre-line. ---, plane free jet (Gutmark & Wygnanski 1976).

$$\bigcirc, \overline{\left(\frac{\partial w'}{\partial z}\right)^2}\frac{h^3}{W_0^2 d}\times 10^{-4}; \quad \triangle, \overline{\left(\frac{\partial u'}{\partial z}\right)^2}\frac{h^3}{W_0^2 d}\times 10^{-4}; \quad \blacktriangledown, \overline{\left(\frac{\partial v'}{\partial z}\right)^2}\frac{h^3}{W_0^2 d}\times 10^{-4}.$$

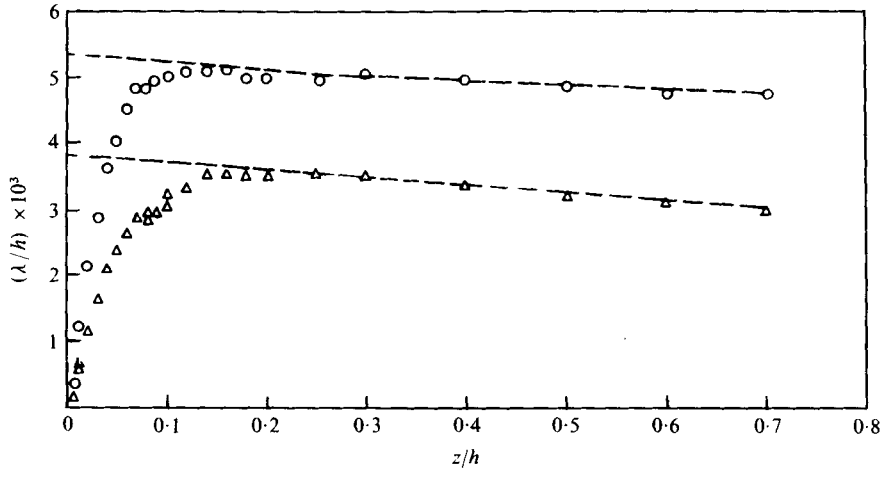

FIGURE 9. Longitudinal and lateral microscales along the jet centre-line. $\bigcirc, \lambda_z$; $\triangle, \lambda_x$; ---, plane free jet (Gutmark & Wygnanski 1976).

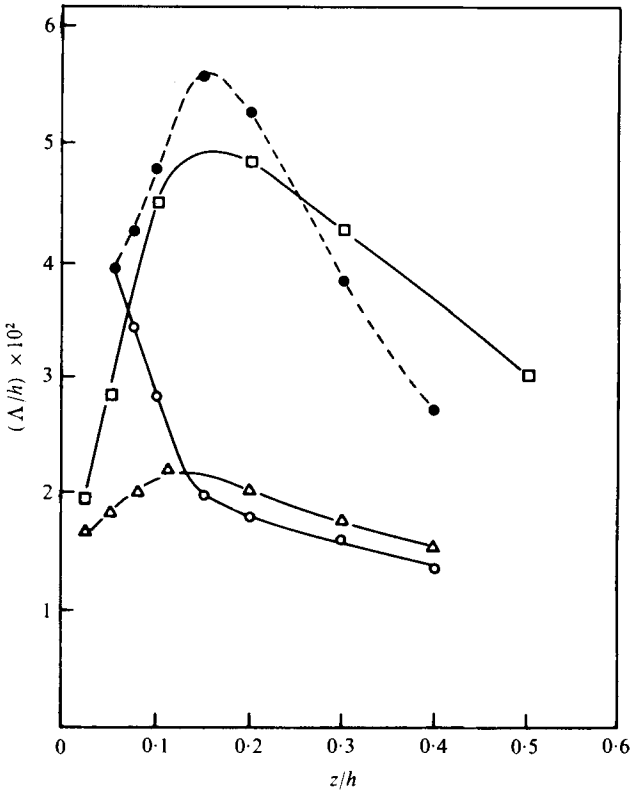

FIGURE 10. The three integral scales along the jet centre-line. □, Λ_z; ○, Λ_x, positive area; ●, Λ_x, positive area + |negative area|; △, Λ_y.

Therefore the time scales are of order unity. Thus one does not expect that the rapid-distortion model can be applied to predict the overall turbulence level because a large fraction of the available energy will be exchanged among the eddies themselves rather than between the eddies and the mean flow.

We shall attempt to compare the amplification rates of the lowest frequencies with decreasing distance from the plate. Because of the different definitions of spectra in the present work and Hunt's paper, the spectrum shown in figure 6 (*a*) has to be divided by the local mean velocity for consistency with the notation of Hunt. If we normalize all the data by the spectrum at $z/h = 0{\cdot}2$ then the local amplification rate becomes

$$A = \overline{W}_M^{-1} F_z(St = 2{\cdot}6)/\overline{W}_M^{-1} F_z(St = 2{\cdot}6)]_{z/h=0{\cdot}2}.$$

The quantity A may be directly compared with the calculations of Hunt (his figure 13) provided that the length scale at the beginning of the stagnation region ($z = 0{\cdot}2h$) is stretched by a factor of 10. The comparison is not expected to work in the immediate vicinity of the plate or for $z/h \gg 0{\cdot}2$ because both regions are outside the range for which the model applies (figure 11).

3.8. *Triple velocity products*

There are 27 possible triple velocity products but only 10 of these are independent. Three of them vanish on the jet axis owing to antisymmetry ($\overline{w'^2u'}$, $\overline{u'^3}$, $\overline{u'v'^2}$). Four others vanish owing to two-dimensionality ($\overline{u'v'w'}$, $\overline{w'^2v'}$, $\overline{u'^2v'}$, $\overline{v'^3}$). The three

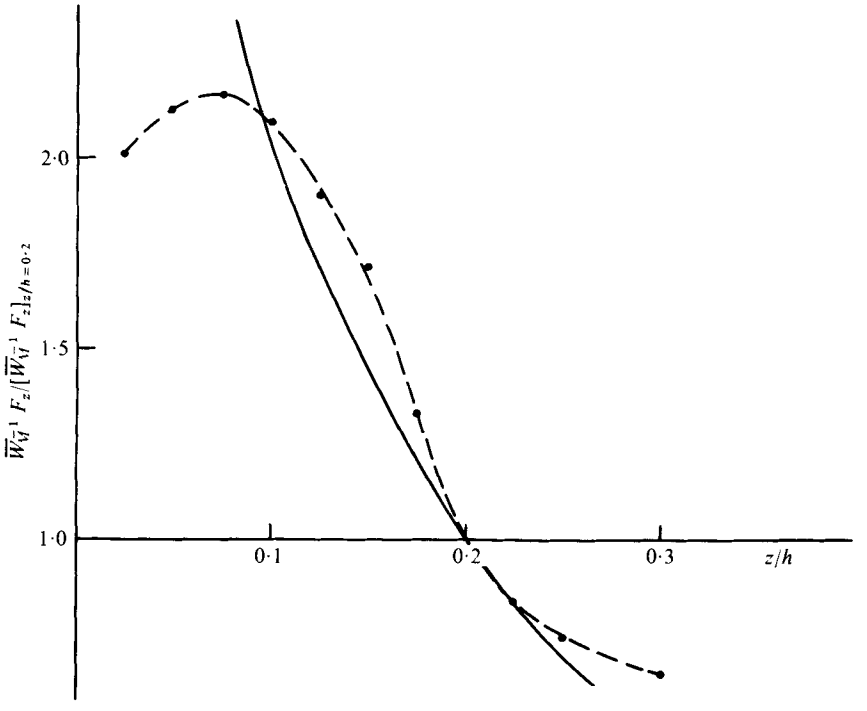

FIGURE 11. The amplitude of the lowest frequency part of w' in the stagnation region. ●, measured at $S = 2{\cdot}6$; ——, from Hunt's figure 13.

remaining components were measured along the jet centre-line and were found to have vanishingly small values. The three antisymmetric components may, in principle, give rise to some turbulent diffusion if their derivatives in the x direction are finite. However, measurements showed these derivatives to be vanishingly small as well. Thus no significant turbulent diffusion exists on the jet's centre-line.

3.9. *The turbulent energy balance*

Energy is normally transferred in turbulent flows from large eddies to smaller ones. In the impinging jet there is an appreciable transfer of energy among the three principal directions. On the jet centre-line turbulent energy is produced by the mean flow only in the w' direction. There is no net production of v' and there is negative production of u'. Therefore a considerable part of the u' energy is likely to be transferred from w' by pressure–velocity interaction. A better understanding of these processes can be gained from the turbulent energy balance of the different components. The transport equations for the energy components in the steady flow are well known and appear in many books (e.g. Hinze 1975, chap. 1).

On the plane of symmetry of a two-dimensional jet they reduce to

$$\underset{\text{convection}}{\frac{\overline{W_M}}{2}\frac{\partial\overline{w'^2}}{\partial z}} = \underset{\text{viscous diffusion}}{\frac{\nu}{2}\left(\frac{\partial^2\overline{w'^2}}{\partial z^2}+\frac{\partial^2\overline{w'^2}}{\partial x^2}\right)} \underset{\text{production}}{-\overline{w'^2}\frac{\partial\overline{W_M}}{\partial z}} \underset{\text{turbulent diffusion}}{-\frac{1}{2}\frac{\partial\overline{w'^3}}{\partial z}-\frac{1}{2}\frac{\partial\overline{u'w'^2}}{\partial x}} -\frac{1}{\rho}\frac{\partial\overline{p'w'}}{\partial z}$$

$$\underset{\text{dissipation}}{-\nu\left[\overline{\left(\frac{\partial w'}{\partial z}\right)^2}+\overline{\left(\frac{\partial w'}{\partial x}\right)^2}+\overline{\left(\frac{\partial w'}{\partial y}\right)^2}\right]} \underset{\text{redistribution}}{+\frac{1}{\rho}\overline{p'\frac{\partial w'}{\partial z}}} \quad \text{in the } z \text{ direction,}$$

$$\underset{\text{convection}}{\frac{\overline{W_M}}{2}\frac{\partial\overline{u'^2}}{\partial z}} = \underset{\text{viscous diffusion}}{\frac{\nu}{2}\left(\frac{\partial^2\overline{u'^2}}{\partial z^2}+\frac{\partial^2\overline{u'^2}}{\partial x^2}\right)} \underset{\text{production}}{+\overline{u'^2}\frac{\partial\overline{W_M}}{\partial z}} \underset{\text{turbulent diffusion}}{-\frac{1}{2}\frac{\partial\overline{w'u'^2}}{\partial z}-\frac{1}{2}\frac{\partial\overline{u'^3}}{\partial x}} -\frac{1}{\rho}\frac{\partial\overline{p'u'}}{\partial x}$$

$$\underset{\text{dissipation}}{-\nu\left[\overline{\left(\frac{\partial u'}{\partial z}\right)^2}+\overline{\left(\frac{\partial u'}{\partial x}\right)^2}+\overline{\left(\frac{\partial u'}{\partial y}\right)^2}\right]} \underset{\text{redistribution}}{+\frac{1}{\rho}\overline{p'\frac{\partial u'}{\partial x}}} \quad \text{in the } x \text{ direction,}$$

$$\underset{\text{convection}}{\frac{\overline{W_M}}{2}\frac{\partial\overline{v'^2}}{\partial z}} = \underset{\text{viscous diffusion}}{\frac{\nu}{2}\left(\frac{\partial^2\overline{v'^2}}{\partial z^2}+\frac{\partial^2\overline{v'^2}}{\partial x^2}\right)} \underset{\text{turbulent diffusion}}{-\frac{1}{2}\frac{\partial\overline{w'v'^2}}{\partial z}-\frac{1}{2}\frac{\partial\overline{u'v'^2}}{\partial x}}$$

$$\underset{\text{dissipation}}{-\nu\left[\overline{\left(\frac{\partial v'}{\partial z}\right)^2}+\overline{\left(\frac{\partial v'}{\partial x}\right)^2}+\overline{\left(\frac{\partial v'}{\partial y}\right)^2}\right]} \underset{\text{redistribution}}{+\frac{1}{\rho}\overline{p'\frac{\partial v'}{\partial y}}} \quad \text{in the } y \text{ direction.}$$

The total turbulent energy balance equation is

$$\underset{\text{convection}}{\overline{W_M}\frac{\partial\overline{q^2}}{\partial z}} = \underset{\text{viscous diffusion}}{\nu\left(\frac{\partial^2\overline{q^2}}{\partial z^2}+\frac{\partial^2\overline{q^2}}{\partial x^2}\right)} \underset{\text{production}}{-\frac{\partial\overline{W_M}}{\partial z}(\overline{w'^2}-\overline{u'^2})} \underset{\text{turbulent diffusion}}{-\left(\frac{\partial\overline{w'q^2}}{\partial z}+\frac{\partial\overline{u'q^2}}{\partial x}\right)} \underset{\text{pressure diffusion}}{-\frac{1}{\rho}\left(\frac{\partial\overline{p'w'}}{\partial z}+\frac{\partial\overline{p'u'}}{\partial x}\right)} \underset{\text{dissipation}}{-\epsilon}.$$

The turbulent and viscous diffusion terms are vanishingly small.

Because isotropy cannot be assumed in the present flow, another approximation has to be made in calculating the viscous dissipation terms. From previous experiments in an axisymmetric jet (Wygnanski & Fiedler 1969), it was established that there is approximately a constant ratio between the diagonal and off-diagonal terms $\overline{(\partial u_i'/\partial x_j)^2}$ $(i,j = 1, 2, 3)$, which leads to the assumption that the sums of every row and column are equal. The sum of the three terms $\overline{(\partial u_i/\partial z)^2}$ $(i = 1, 2, 3)$ measured represents the sum of one column in the matrix so the sums of the other columns are assumed to be equal to it. The pressure–velocity correlation terms are the only totally unknown quantities and constitute the balance of the equations.

The energy budgets for each of the three components of the velocity fluctuations are given in figures 12(*a*)–(*c*) and the total energy balance in figure 13. The corresponding energy balances for the free jet given by Gutmark & Wygnanski are shown in these figures as well. Some interesting features of the flow are the following.

(i) The convection is very similar to that for the free jet upstream of $0{\cdot}2\,h$ from the plate. At this point the convection of u' increases rapidly. A similar increased convection may be seen for w' and v' at a distance of $0{\cdot}1h$ from the plate. The point of maximum convection corresponds to the place where the two-point correlation curves start to deviate from a self-preserving shape.

(ii) The production shows some unusual behaviour. Production of w' is always finite on the centre-line. This is a consequence of the normal stresses, which are generated by

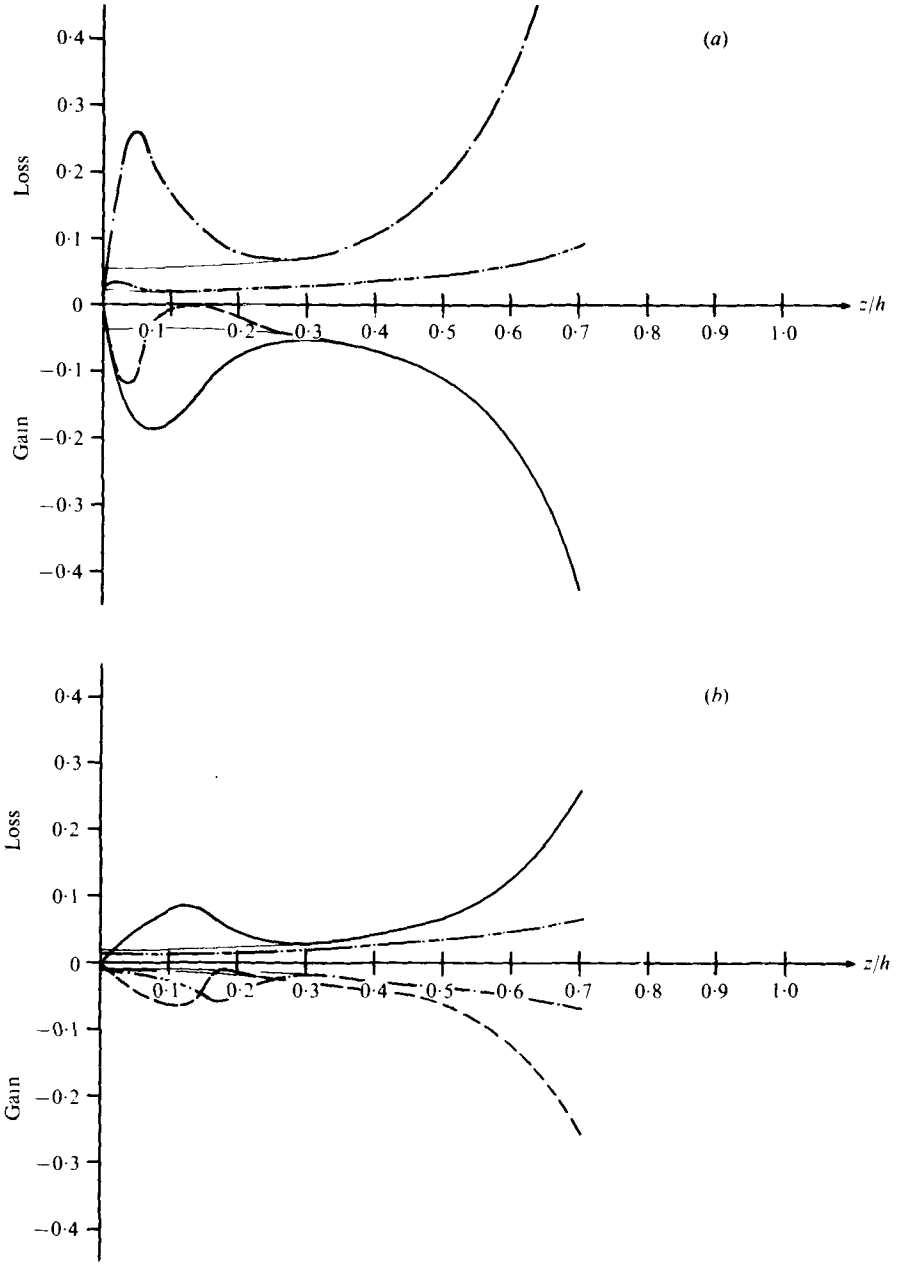

FIGURES 12 (*a*,*b*). For legend see facing page.

the strong deceleration, while the shear stress vanishes owing to symmetry. As the wall is approached and the velocity gradient increases, the production term increases very rapidly before it decays to zero at the wall. The production of u' is similar in magnitude but opposite in sign to that of w' because $\partial W/\partial z = -\partial U/\partial x$ and the u' distribution resembles the w' distribution. There is no energy production in the transverse com ponent v' because there is no mean shear in this direction.

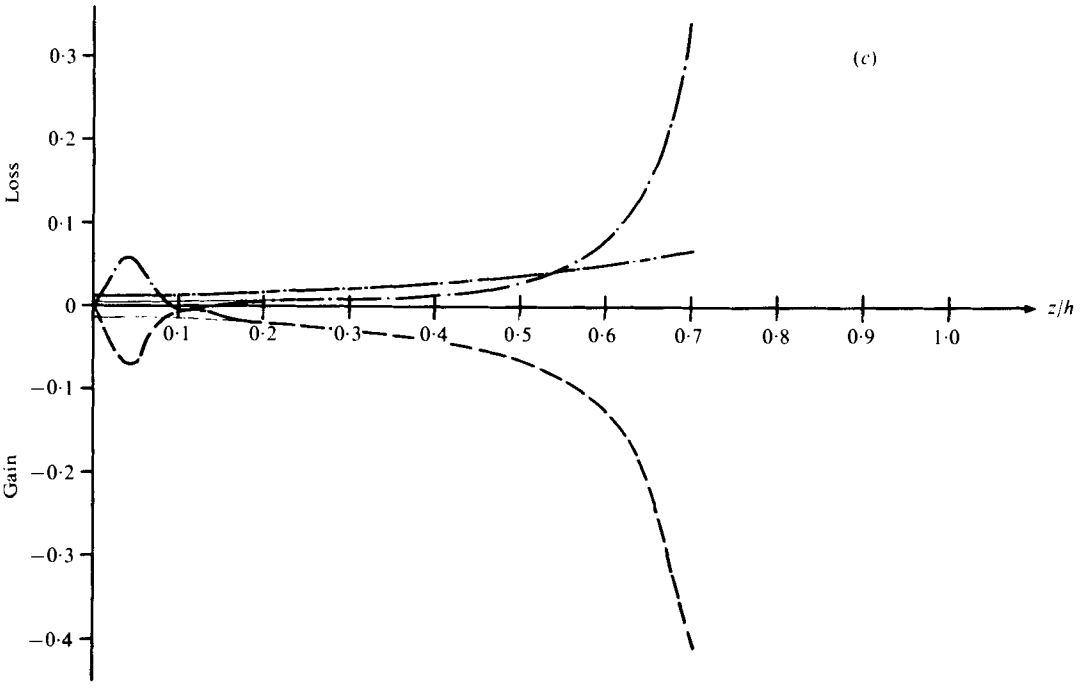

FIGURE 12. Energy balance for (*a*) longitudinal, (*b*) lateral and (*c*) transverse velocity fluctuations along the jet centre-line. ——, production; – – –, convection; —·–·—, dissipation; —·—, diffusion and redistribution; ——, free jet.

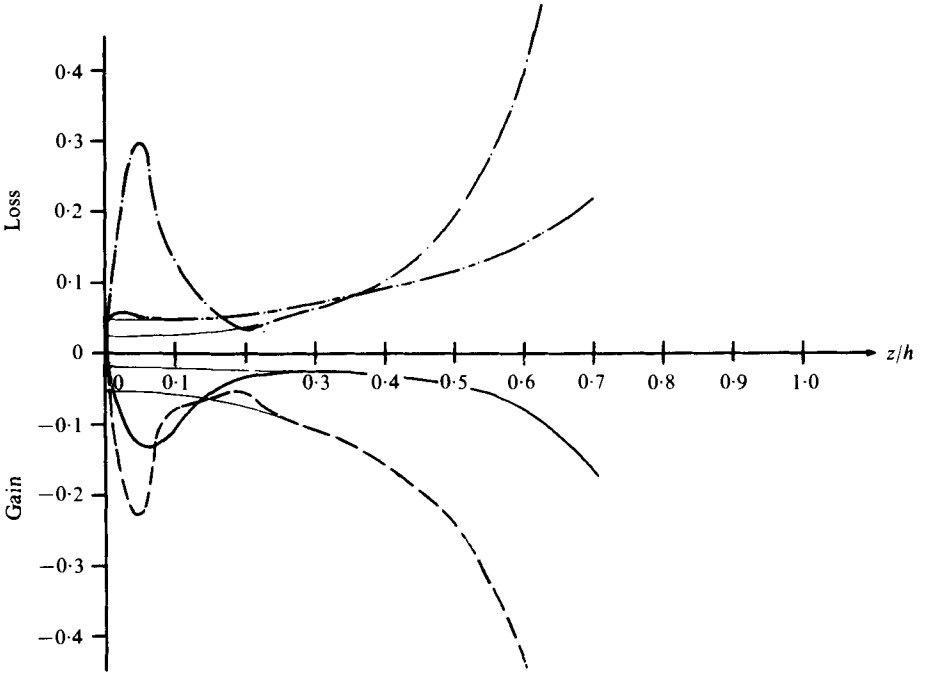

FIGURE 13. Total energy balance along the jet centre-line. ——, production; – – –, convection; —·–·—, dissipation; —·—, diffusion; ——, free jet.

(iii) The dissipation curve is quite regular and similar to the dissipation in the free jet up to a distance of about $0{\cdot}1\,h$ from the wall, where it is slightly augmented. On the wall only three velocity derivatives have non-zero values, namely $\overline{(\partial u'/\partial z)^2}$, $\overline{(\partial w'/\partial z)^2}$ and $\overline{(\partial v'/\partial z)^2}$. Since it is very difficult to measure these terms in the immediate vicinity of the wall, the energy dissipation was estimated by extrapolating the measured curves.

(iv) The turbulent diffusion is negligible on the jet centre-line.

(v) The remaining terms are the pressure–velocity interactions, whose main role is to redistribute the energy among the different velocity components. One may observe how energy is transferred from the w' component to the u' component by this mechanism.

4. Conclusions

A two-dimensional jet impinging onto a plate which is normal to the plane of symmetry of the jet is not affected by the presence of the plate over 75 % of the distance between the nozzle and the plate ($z/h \leqslant 0{\cdot}25$). The turbulent properties of the jet change from their equilibrium level even closer to the impingement region

$$(z/h < 0{\cdot}15).$$

The data scale on the distance between the plate and the nozzle because lengths in the self-preserving jet also scale on this distance.

The standing eddy pattern described in papers on stagnation flow was not found in the present investigation. Anistropy is expected in this flow because the straining of the turbulent eddies occurs in a preferred direction. The large eddies gain energy by being stretched by the mean flow while the small ones are dissipated in the process. A neutral scale (frequency) exists for which the two mechanisms balance. The energy of the eddies with such a scale is neither augmented nor attenuated.

REFERENCES

Batchelor, G. K. & Proudman, I. 1954 *Quart. J. Mech. Appl. Math.* **7**, 83.

Bearman, P. W. 1972. *J. Fluid Mech.* **53**, 451.

Beltaos, S. & Rajaratnam, N. 1973 *J. Hydraul. Res.* **11**, 29.

Champagne, F. H. & Sleicher, C. A. 1967 *J. Fluid Mech.* **28**, 177.

Donaldson, C. duP., Snedeker, R. S. & Margolis, D. P. 1971 *J. Fluid Mech.* **45**, 477.

Gardon, R. & Akfirat, J. C. 1965 *Int. J. Heat Mass Transfer* **8**, 1261.

Gutmark, E. & Wygnanski, I. 1976 *J. Fluid Mech.* **73**, 465.

Heskestad, G. 1965 *J. Appl. Sci. Res.* A **7**, 293.

Hinze, J. O. 1975 *Turbulence*, 2nd edn. McGraw-Hill.

Hunt, J. C. R. 1973 *J. Fluid Mech.* **61**, 625.

Kestin, J. & Maeder, P. F. 1957 *N.A.C.A. Tech. Note* no. 4018.

Sadeh, W. Z., Sutera, S. P. & Maeder, P. F. 1970 *Z. angew. Math. Phys.* **21**, 699.

Schauer, J. J. & Eustis, R. H. 1963 The flow development and heat transfer characteristics of plane turbulent impinging jets. *Stanford Univ. Tech. Rep.* no. 3.

Smith, M. C. & Kuethe, A. M. 1966 *Phys. Fluids* **9**, 2337.

Sutera, S. P., Maeder, P. F. & Kestin, J. 1963 *J. Fluid Mech.* **16**, 497.

Wygnanski, I. & Fiedler, H. 1969 *J. Fluid Mech.* **38**, 577.